9-1-2023

Low-frequency laboratory measurements of the elastic properties of solids using a distributed acoustic sensing system

Vassily Mikhaltsevitch

Maxim Lebedev
Edith Cowan University

Roman Pevzner

Alexey Yurikov

Konstantin Tertyshnikov

10.1016/j.jrmge.2023.05.002
Mikhaltsevitch, V., Lebedev, M., Pevzner, R., Yurikov, A., & Tertyshnikov, K. (2023). Low-frequency laboratory measurements of the elastic properties of solids using a distributed acoustic sensing system. Journal of Rock Mechanics and Geotechnical Engineering, 15(9), 2330-2338. https://doi.org/10.1016/j.jrmge.2023.05.002

Journal of Rock Mechanics and Geotechnical Engineering 15 (2023) 2330–2338

Contents lists available at ScienceDirect

Journal of Rock Mechanics and Geotechnical Engineering

journal homepage: www.jrmge.cn

Full Length Article

Low-frequency laboratory measurements of the elastic properties of solids using a distributed acoustic sensing system

Vassily Mikhaltsevitch [a,*], Maxim Lebedev [a,b], Roman Pevzner [a], Alexey Yurikov [a], Konstantin Tertyshnikov [a]

[a] Curtin University, GPO Box U1987, Perth, WA 6845, Australia
[b] Centre for Sustainable Energy and Resources, Edith Cowan University, 270 Joondalup Dr, Joondalup, WA 6027, Australia

ARTICLE INFO

Article history:
Received 7 September 2022
Received in revised form
18 April 2023
Accepted 15 May 2023
Available online 8 June 2023

Keywords:
Elasticity and anelasticity
Acoustic properties
Fourier analysis
Wave propagation

ABSTRACT

In recent decades, low-frequency (LF) experiments based on the forced-oscillation (FO) method have become common practice in many rock physics laboratories for measuring the elastic and anelastic properties of rocks. However, the use of the electronic displacement sensors in traditional acquisition systems of FO devices such as conventional capacitive transducers or strain gauges seriously limits both the efficiency and productivity of LF measurements, and, due to the limited contact area of the displacement sensors with a sample under test, increases the requirements for sample homogeneity. In this paper, we present the first results obtained in the development of a new laboratory method elaborated to measure the elastic properties of solids. The method is a further development of the FO method where traditional data acquisition is replaced by acquisition based on fiber-optic distributed acoustic sensing (DAS) technology. The new method was tested in a laboratory study using two FO setups designed for measurements under uniaxial and confining pressures. The study was carried out on a sample made from polymethyl methacrylate (PMMA) and an aluminium standard, first under uniaxial pressure at FO frequencies of 1, 10, 30, 60 and 100 Hz, and then under confining pressure at an FO frequency of 1 Hz. Both uniaxial and confining pressures were equal to 10 MPa, and the strain in the PMMA sample in all measurements did not exceed 4×10^{-8}. The performance of DAS acquisition was compared with the measurements conducted at a strain of 1×10^{-6} using the traditional FO method based on the use of semiconductor strain gauges and the ultrasonic method. The results of the DAS measurements are in good agreement with the FO measurements carried out using semiconductor strain gauges and with the literature data.

1. Introduction

In the last years, the forced-oscillation (FO) method became a popular alternative to the traditional ultrasonic measurements of the elastic and anelastic properties of solids (Adelinet et al., 2010; Jackson et al., 2011; Subramaniyan et al., 2014; Ògúnsànmì, 2021), which remain the most common laboratory practices for studying the elastic properties of rocks at present. The increasing spread of the FO method is mainly caused by the match of the operating frequencies of the FO apparatuses with the frequencies of the field seismic experiments, which significantly simplifies the interpretation of measurement data of fluid-saturated rocks (Mikhaltsevitch et al., 2014a). Another important reason of the widespread use of the FO method in present-day laboratory studies is related to the opportunity provided by this method to easily control the level of dynamic strain in a sample under test (Mikhaltsevitch et al., 2021). As was reported in a number of studies (Gordon and Davis, 1968; Mavko, 1979; Winkler et al., 1979), frictional attenuation between grain contacts in rocks becomes negligible if amplitudes of strains caused by acoustic waves are less than 1×10^{-6}. This strain amplitude limit is adequate to the seismic measurements in real fields and imposes one of the most important restrictions on any laboratory measurements of the elastic and anelastic properties of rocks. However, due to the complexity of determining the amplitude of the strains caused by an ultrasonic wave, in the vast majority of laboratory ultrasonic measurements, these amplitudes are

* Corresponding author.
E-mail address: V.Mikhaltsevitch@curtin.edu.au (V. Mikhaltsevitch).
Peer review under responsibility of Institute of Rock and Soil Mechanics, Chinese Academy of Sciences.

https://doi.org/10.1016/j.jrmge.2023.05.002

not controlled, which often leads to overestimated values of the measured elastic moduli (Nourifard and Lebedev, 2019).

Despite the fact that the FO method eliminates the main drawbacks of ultrasonic methods, this method also has a number of disadvantages, primarily related to the use of traditional electronic sensors for strain measurements, such as capacitive displacement transducers or strain gauges, which leads to a long measurement time and strict requirements for the homogeneity of the sample under test imposed by the limited contact area of the electronic sensors with the sample.

Let us note here that one of the growing trends in the development of modern scientific and industrial technologies for controlling and monitoring various parameters of ongoing processes is the transition from electronic measuring systems and sensors to the devices based on fiber-optic sensing. Fiber-optic sensors are able to meet the stringent requirements of modern research and industry for reliability, noise immunity, operating conditions and measurement accuracy (Udd, 1995). Fiber-optic sensing technologies have been evolving over the past 30 years and have led to the development of new instruments for such engineering applications as structural health monitoring, leak detection in pipelines, smart surveillance, chemical analysis, temperature and vibration sensing (Udd, 1995; Barrias et al., 2016; Tejedor et al., 2018; Lu et al., 2019a, b; Fernandez-Ruiz et al., 2019; Zhang and Das, 2021). At the same time, there was also a widespread introduction of fiber-optic sensors in various areas of geophysics. Distributed fiber-optic sensors replaced electronic gauges in monitoring pressure and temperature in unconventional reservoirs and enhanced hydrocarbon recovery (Rehman and Mendez, 2012), as well as in the detection of acoustic events during time-lapse seismic reservoir monitoring, near-surface and borehole geophysical surveys (Baldwin, 2014; Fenta et al., 2021; Sidenko et al., 2021; Pevzner et al., 2022).

The distributed fiber-optic sensors have been successfully used in a number of geotechnical engineering applications such as ground settlement and soil reinforcement monitoring (Mohamad et al., 2011; Linker and Klar, 2015; Xu and Yin, 2016; Rossi et al., 2022), landslide and rock deformation control (Suo et al., 2016; Damiano et al., 2017; Liu et al., 2020), geotechnical infrastructure health monitoring (Ohno et al., 2001; Murayama et al., 2003; Fan et al., 2018), as well as reconstruction of geotechnical parameters and characterisation of rock formations (Luo et al., 2021; Rossi et al., 2022; Zhu et al., 2022).

The widespread use of distributed fiber-optic sensing in the field of geophysical and geotechnical applications is mainly due to the fact that an optical fiber can be disposed over the entire area or volume of the dimensional object under study and can be used to collect the required information about spatially distributed properties of the object (Gorshkov et al., 2022). The other essential advantages provided by fiber-optic sensors include: corrosion resistance, high sensitivity over long distances, good resolution and accuracy, immunity to high voltage environments and electromagnetic interference, high robustness, durability, adaptability to harsh environmental conditions, light weight, as well as the low cost for long-term operations and for monitoring of large areas/volumes (Habel and Krebber, 2011; Xie et al., 2021; Gorshkov et al., 2022; Ma et al., 2023).

Considering that the interpretation of the results of laboratory studies is often limited by the discrepancy between the instruments used in real geotechnical and geophysical practice and laboratory instruments, it seems highly desirable to explore the possibility of using fiber-optic sensing in laboratory measurements.

Recently, Yurikov et al. (2021) reported the first application of fiber-optic distributed acoustic sensing (DAS) in the FO laboratory measurements of the elastic properties of solid materials, where the DAS system replaced a data acquisition system based on traditional electronic sensors. The main advantages of using DAS systems are associated with very high strain sensitivity (to 10^{-12}), high signal-to-noise ratio (which is a consequence of the immunity of fiber-optic sensors to electromagnetic interference), shorter measurement time, and large frequency range. It is especially important to note that in the case of winding an optical fiber along the entire measured sample, the experimenter gets the opportunity to register a signal from any section of the sample of arbitrary thickness, which can vary from a fraction of a millimetre to the entire length of the sample. However, despite the demonstration of the highest sensitivity of DAS systems when measuring strains in solids, Yurikov et al. (2021) did not propose a methodology for determining the main parameters of elasticity of the tested samples.

In this paper, we present a new approach to the study of the elastic properties of solids that includes a combination of the FO measurements with DAS carried out under both uniaxial and confining pressures. It is shown that the FO measurements at uniaxial and confining pressures of the same value enable to determine all the main elastic parameters of solids, such as Young's modulus, bulk modulus, shear modulus, and Poisson's ratio. In our study, the experiments were conducted on two joint samples, an aluminium standard and a PMMA sample, first at uniaxial pressure and then at confining pressure. Both pressures were equal to 10 MPa. The results of the FO measurements with DAS are compared with the data obtained for the same sample and standard using the traditional FO method based on strain gauges and the ultrasonic method.

2. Experimental setups, specimens and operation

The laboratory study was performed using three low-frequency (LF) experimental setups and a standard ultrasonic system described in detail in Mikhaltsevitch et al. (2014b).

The first LF setup with the DAS acquisition system is based on a uniaxial apparatus with longitudinal type of the forced oscillations (Mikhaltsevitch et al., 2021). The setup is designed to measure the ratio of the radial strain amplitudes detected in a test sample and a standard with known elastic parameters. The schematics and mechanical assembly of this setup are presented in Fig. 1.

The second LF setup was designed to measure the bulk moduli of elastic materials when the confining pressure is periodically modulated by an electric pump. This setup is demonstrated in Fig. 2.

The third LF setup is a standard uniaxial FO apparatus with the acquisition system based on strain gauges (Mikhaltsevitch et al., 2021). This setup enables to measure Poisson's ratio and Young's modulus. The schematics and mechanical assembly of this setup are presented in Fig. 3a and b, correspondingly.

The steel frame used in the uniaxial LF experiments was also used for the ultrasonic setup. In this setup, the central column formed by the units located inside the steel frame (Fig. 3b) was replaced by the set of units displayed in Fig. 4. The ultrasonic transducers were placed inside steel endcaps where they were fixed to their position facing the ends of the sample by steel springs. To generate and record the ultrasonic pulses, we used a Pulser-and-Receiver System 5077 PR, Olympus, and a digital oscilloscope TDS3034C, Tektronix.

The measurements were conducted on two specimens, an aluminium standard and a PMMA sample of the same diameter, equal to 38 mm; the lengths of the standard and sample are 95 mm and 100 mm, respectively. The density of the aluminium standard is 2700 kg/m^3 and the density of the PMMA sample is equal to 1884 kg/m^3. There are 252 turns of fiber wound in the center of each specimen, which corresponds to 30 m of fiber length and

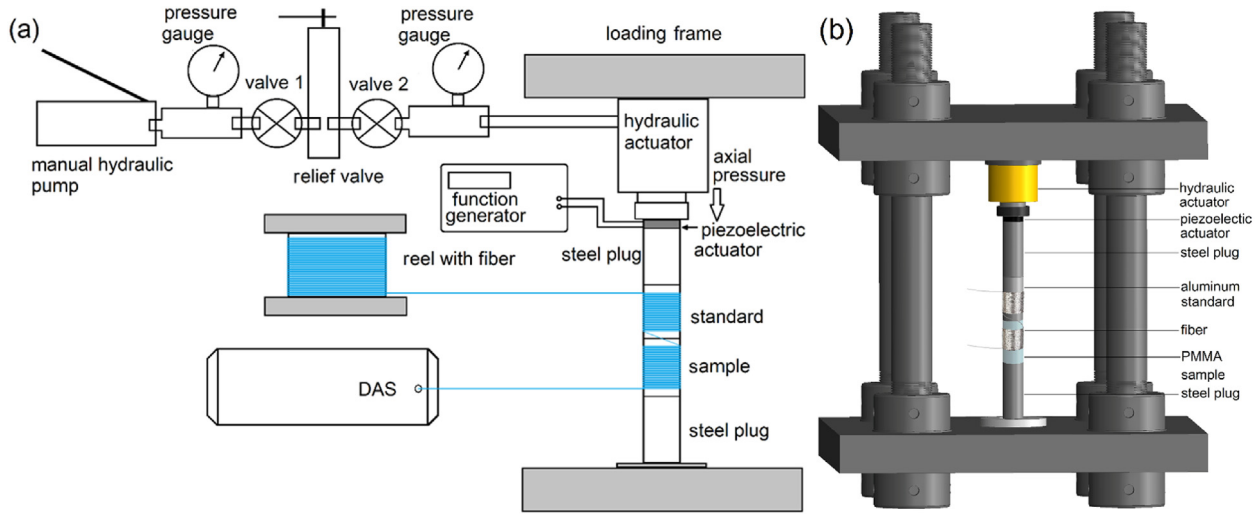

Fig. 1. (a) Schematic of the FO uniaxial setup with DAS, and (b) Mechanical assembly of the FO apparatus with a fiber-optic sensor.

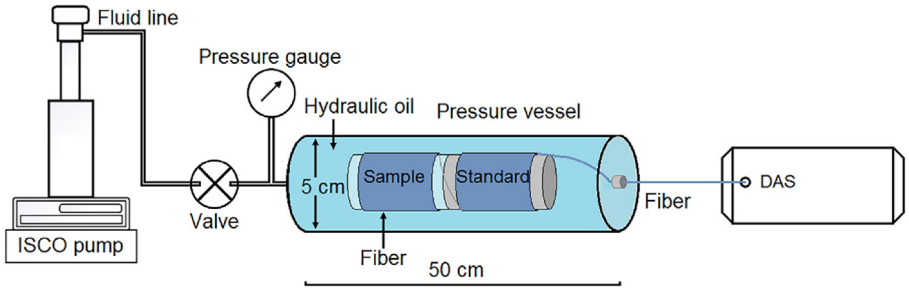

Fig. 2. Diagram of the second experimental setup for the bulk modulus measurements using the DAS system.

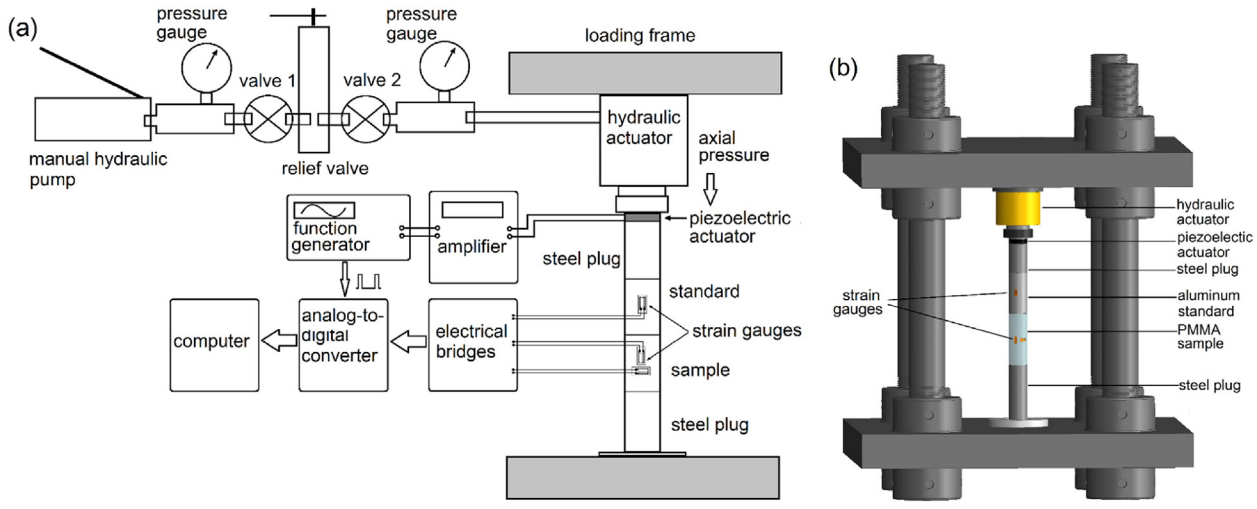

Fig. 3. (a) Schematic of the FO uniaxial setup with strain gauges, and (b) Mechanical assembly of the FO apparatus.

covers 30 mm of each specimen. To ensure tight contact, the fiber was glued to both specimens. The fiber used in our experiments is the bend insensitive F-SM1500–6.4/80 single-mode fiber (Gerich Fiberglass Inc.) with a diameter of 80 μm and an attenuation of 0.31 dB/km at an operating wavelength of 1550 nm.

Let us consider these setups and their operation in more detail.

2.1. Uniaxial low-frequency setup with DAS data acquisition system

The uniaxial setup with the acquisition system based on DAS is presented in Fig. 1a. The mechanical part of this setup includes an assembly comprising the frame formed by two steel plates connected by four steel poles and a set of units placed in the center of the frame as shown in Fig. 1b. The set includes a hydraulic actuator,

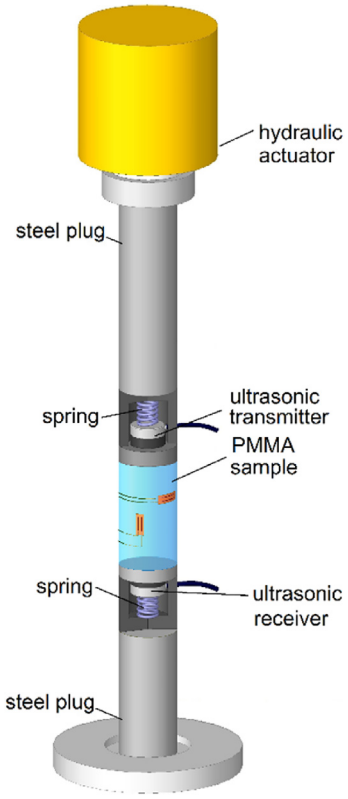

Fig. 4. Configuration of the unit set for ultrasonic measurements.

a PICA stack piezoelectric actuator P-035.10P (Physik Instrumente GmbH & Co. KG) with a resonant frequency of 51 kHz, an aluminium calibration standard, a PMMA sample, and two steel plugs, one of which is located between the piezoelectric actuator and the standard and the second one placed between the PMMA sample and the lower steel plate (Fig. 1b). The hydraulic actuator (model RCS201, Enerpac) is connected via fluid lines with a manual hydraulic pump (model P392, Enerpac) that applies a longitudinal static force to the sample and the standard, as shown in Fig. 1a.

In this setup, the fiber is wound around the standard and the sample along their circumference. As was shown in Yurikov et al. (2021), in this configuration, DAS only measures the radial components of the strain rate in the sample and standard, which restricts our capability to directly obtain the elastic moduli, but allows us to estimate the strain ratio between the sample and standard.

The operation of this setup can be described as follows. The multilayer piezoelectric actuator transforms the periodic sinusoidal voltage, provided by a function generator (Agilent 33220A), into mechanical stress, which causes axial and radial dynamic strains in the aluminium standard and tested sample. The dynamic strains in the specimens are measured by a DAS interrogator unit (Silixa iDASv2) connected to the fiber wound around the specimens.

The iDASv2 interrogator unit uses Rayleigh backscatter in fiber from a coherent light source, such as a laser, to measure changes in strain over the given length of the fiber (so-called 'gauge length') at regular time intervals using phase-sensitive optical time-domain reflectometry (Becker and Coleman, 2019). The unit registers the change in strain, derived from the difference between the phases of the backscattered signals separated by a window of the gauge length, the central position of which ('channel') is gradually shifted by a constant increment ('channel spacing') from the beginning to the end of fiber. The DAS response measured by the iDAS v2 unit is proportional to (Daley et al., 2016):

$$\frac{\partial \varepsilon(z_i)}{\partial t} = \frac{\partial}{\partial t}\left(\frac{\partial u(z_i)}{\partial z}\right) \tag{1}$$

where ε and u are, respectively, the dynamic strain and displacement of the fiber at the point z_i corresponding to the location of the i-th channel; dz is the gauge length; and dt is the time interval between the measurements. In our experiments, the time interval between the measurements is 1 ms, the gauge length and the channel spacing are equal to 10 m and 1 m, respectively.

The configuration of the fiber winding, as shown in Fig. 1, allows us to register only radial strains, the amplitudes of which can be presented as follows:

$$\varepsilon_{\mathrm{rad}}^{\mathrm{st}} = \nu^{\mathrm{st}}\varepsilon_{\mathrm{ax}}^{\mathrm{st}}, \varepsilon_{\mathrm{rad}} = \nu\varepsilon_{\mathrm{ax}} \tag{2}$$

where $\varepsilon_{\mathrm{ax}}$ and $\varepsilon_{\mathrm{ax}}^{\mathrm{st}}$ are the amplitudes of axial strains in the sample and standard, respectively; and ν^{st} and ν are the Poisson's ratios of the standard and sample, respectively. Since the sample and standard diameters are equal to each other, the stress σ applied to both specimens is the same:

$$\sigma = E\varepsilon_{\mathrm{ax}} = E^{\mathrm{st}}\varepsilon_{\mathrm{ax}}^{\mathrm{st}} \tag{3}$$

which yields

$$\varepsilon_{\mathrm{ax}} = \varepsilon_{\mathrm{ax}}^{\mathrm{st}}\frac{E^{\mathrm{st}}}{E} \tag{4}$$

where E^{st} and E are the Young's moduli of the standard and sample, respectively.

Thus, the first uniaxial setup can be used to measure the ratio of the radial strains in the sample and aluminium standard:

$$R_{\mathrm{u}} = \frac{\varepsilon_{\mathrm{rad}}}{\varepsilon_{\mathrm{rad}}^{\mathrm{st}}} = \frac{\nu}{\nu^{\mathrm{st}}}\frac{\varepsilon_{\mathrm{ax}}}{\varepsilon_{\mathrm{ax}}^{\mathrm{st}}} = \frac{\nu}{\nu^{\mathrm{st}}}\frac{E^{\mathrm{st}}}{E} \tag{5}$$

Eq. (5) contains two unknown parameters, ν and E, that cannot be determined from one expression. However, by carrying out additional experiments with oscillating confining pressure, it is possible to determine ν and E, and, as a result, the shear and bulk moduli.

2.2. Confining setup with DAS data acquisition system

The second experimental setup was designed to measure the bulk moduli of specimens using oscillating confining pressure (Fig. 2). The static component of the confining pressure and its oscillating part of a triangular form were controlled by a syringe pump (model 260D, Teledyne Isco). The LF bulk moduli of the PMMA sample and the aluminium standard can be derived from the ratio of confining pressure oscillations ΔP_{c} to volumetric strain:

$$K_{\mathrm{st}} = -\frac{\Delta P_{\mathrm{c}}}{\varepsilon_{\mathrm{V}}^{\mathrm{st}}} \tag{6}$$

$$K = -\frac{\Delta P_{\mathrm{c}}}{\varepsilon_{\mathrm{V}}} \tag{7}$$

where $\varepsilon_{\mathrm{V}}^{\mathrm{st}}$ and ε_{V} are the volumetric strains corresponding to the deformation of the standard and sample, respectively. The volumetric strain can be obtained from the following relations:

$$\varepsilon_V = 2\varepsilon_{rad} + \varepsilon_{ax}, \varepsilon_V = 2\varepsilon_{rad}^{st} + \varepsilon_{ax}^{st} \tag{8}$$

where ε_{rad} and ε_{ax} are the radial and axial strains in the sample, and ε_{rad}^{st} and ε_{ax}^{st} are the radial and axial strains in the standard.

However, taking into account the isotropy of the sample and standard, the volumetric strains ε_V^{st} and ε_V can be found as

$$\varepsilon_V^{st} = 3\varepsilon_{rad}^{st}, \varepsilon_V = 3\varepsilon_{rad} \tag{9}$$

Therefore, dividing Eq. (6) by Eq. (7), we obtain

$$\frac{K_{st}}{K} = \frac{\varepsilon_{rad}}{\varepsilon_{rad}^{st}} \tag{10}$$

Since the bulk modulus of the standard is known from ultrasonic measurements, the bulk modulus of the sample can be found from the following relation:

$$K = K_{st}\frac{\varepsilon_{rad}^{st}}{\varepsilon_{rad}} \tag{11}$$

Combining the results of the uniaxial measurements with the data obtained in the experiments with confining pressure oscillations, we can find all elastic parameters of the sample.

The bulk moduli K_{st} and K can be presented as

$$K = \frac{E}{3(1-2\nu)} \tag{12}$$

$$K_{st} = \frac{E_{st}}{3(1-2\nu_{st})} \tag{13}$$

In accordance with Eqs. (6), (7), (9), (12) and (13), the ratio of K_{st} to K is equal to

$$R_c = \frac{K_{st}}{K} = \frac{\varepsilon_{rad}}{\varepsilon_{rad}^{st}} = \frac{E^{st}(1-2\nu)}{E(1-2\nu_{st})} \tag{14}$$

The ratio of Eq. (14) to Eq. (5) is completely determined by Poisson's ratios ν and ν_{st}:

$$\frac{R_c}{R_u} = \frac{\nu^{st}(1-2\nu)}{\nu(1-2\nu_{st})} \tag{15}$$

which yields the expression for Poisson's ratio ν:

$$\nu = \left[\frac{R_c}{R_u}\left(\frac{1}{\nu^{st}} - 2\right) + 2\right]^{-1} \tag{16}$$

Substituting Eq. (16) into Eq. (5) gives the expression for Young's modulus of the sample:

$$E = \frac{\nu}{\nu^{st}}\frac{E^{st}}{R_u} = \frac{E^{st}}{R_c + 2\nu^{st}(R_u - R_c)} \tag{17}$$

The shear modulus μ can be found from the known Poisson's ratio and Young's modulus as

$$\mu = \frac{E}{2(1+\nu)} \tag{18}$$

2.3. Uniaxial low-frequency setup with strain gauges

The schematic and mechanical assembly of the uniaxial setup with the acquisition system based on strain gauges are presented in Fig. 3a and b, correspondingly. The mechanical assembly of the setup is identical to that used in the uniaxial experiments with DAS acquisition.

The dynamic deformation in the aluminium standard and PMMA sample generated by the piezoelectric actuator modulates the conductivity of three semiconductor strain gauges (type KSP-6-350-E4, Kyowa) attached to the standard and sample. One strain gauge is attached to the aluminium standard in the axial direction and two other strain gauges are attached to the sample in axial and circumferential directions. The strain gauges are connected with electric bridges (BCM-1 Wheatstone Bridge, Omega Engineering), which convert the modulated conductivity of the strain gauges into alternated voltage. The voltage is digitized by the analog-to-digital converter (model 100, InstruNet, Omega Engineering) and processed by the computer (Fig. 1a).

Inasmuch as the voltage signals obtained from the axial and circumferential strain gauges coupled to the sample and standard are proportional to the axial and radial strains, the Young's modulus E and Poisson's ratio ν of the sample can be found as

$$E = E^{st}\frac{\varepsilon_{ax}^{st}}{\varepsilon_{ax}} \tag{19}$$

$$\nu = \frac{\varepsilon_{rad}}{\varepsilon_{ax}} \tag{20}$$

Note that Eq. (19) follows directly from Eq. (3). After finding E and ν, the bulk and shear moduli can be found in accordance with Eqs. (12) and (18).

2.4. Uniaxial ultrasonic setup

The frame used in the LF experiments with a modified set of units located between the steel plates was also used in our ultrasonic measurements. The ultrasonic configuration of the set is presented in Fig. 4. The ultrasonic transducers were placed inside steel endcaps where they were pressed by springs against the end butts facing the sample. Ultrasonic pulses with a central frequency of 0.5 MHz were generated and recorded using a pulser-receiver system (5077 PR, Olympus, Ltd.) and a digital oscilloscope (TDS3034C, Tektronix, Ltd.). The ultrasonic P-wave V_P and S-wave V_S velocities were measured using the pulse transmission ("time of flight") technique. Poisson's ratio ν, Young's E, bulk K and shear μ moduli can be found from V_P and V_S using the following relations (Lebedev et al., 2013):

$$\nu = \frac{V_P^2 - 2V_S^2}{2\left(V_P^2 - V_S^2\right)} \tag{21}$$

$$E = \rho V_S^2\frac{3V_P^2 - 4V_S^2}{V_P^2 - V_S^2} \tag{22}$$

$$K = \rho V_P^2 - \frac{4}{3}\rho V_S^2 \tag{23}$$

$$\mu = \rho V_S^2 \tag{24}$$

where ρ is the density of the sample.

The ultrasonic measurements were carried out at a uniaxial pressure of 10 MPa.

3. Experimental procedure

The experimental procedure was organized as follows. First, the PMMA sample and aluminium standard were glued end-to-end. Then the optical fiber was wound in such a way that the winding covered 30 mm of the central part of each specimen. After that, the column, formed by the sample and the standard, with wound fiber was placed into the center of the frame between two steel plates, as shown in Fig. 1b and a set of LF measurements was carried out at frequencies from 1 Hz to 100 Hz under a uniaxial pressure of 10 MPa. The LF measurements were conducted using the Silixa iDASv2 interrogator. At the next stage, the sample and standard with fiber were immerged in hydraulic oil inside a pressure vessel presented by a steel cylinder with an inner chamber 50 cm long and 5 cm in diameter, as demonstrated in Fig. 2. The oil was pressurized to 10 MPa using a syringe pump (model 260D, Teledyne Isco Inc). The measurements of the bulk modulus of the sample were conducted using confining pressure oscillations of triangular shape generated by the syringe pump at a frequency of 1 Hz around a mean pressure of 10 MPa. The amplitude of pressure oscillations ΔP_c was equal to 20 kPa. After completion of the experiments with oscillating confining pressure, the fiber was removed from the sample and standard, and the strain gauges were attached to both specimens as described above. The experimental setup with DAS acquisition was changed to the standard FO uniaxial laboratory setup demonstrated in Fig. 3 and the measurements of the elastic properties of the PMMA sample were conducted at the same pressure and in the same frequency range as the uniaxial measurements with DAS. At the final stage, the PMMA sample was detached from the standard and its elastic properties were measured under an axial pressure of 10 MPa at a frequency of 0.5 MHz using the ultrasonic setup shown in Fig. 4. Finally, considering the strong temperature dependence of the elastic properties of PMMA (see e.g. Tschoegl et al. (2002), Agrawal et al. (2010), and Carneiro and Puga (2018)), note that all measurements were carried out at a temperature of 22 °C.

4. Results of measurements

4.1. Results of the low-frequency measurements with DAS acquisition

An example of the data recorded at a frequency of 60 Hz by the Silixa iDASv2 interrogator unit and the corresponding Fourier transform are presented in Figs. 5 and 6. Fig. 7 demonstrates the strain distribution over the fiber length during the measurements at frequencies of 1 Hz to 100 Hz. The results of the measurements of the ratio of radial strain amplitudes in the sample and the standard R_u obtained using the Silixa iDASv2 interrogator unit are presented in Tables 1 and shown in Fig. 8. Note that the strain amplitudes used to determine R_u were preliminarily averaged over an interval of ±5 mm from the center of each specimen.

In our experiment conducted using the confining setup, the highest frequency of the pressure oscillations achievable using the 260D ISCO pump is 1 Hz. The amplitude of the pressure oscillations used at this frequency was very small and equal to 20 kPa. Fig. 9 shows the data recorded by the Silixa iDASv2 unit. The frequency dependences of the strain amplitudes detected in the standard and the sample are shown in Fig. 10, and the dependence of the strain amplitudes on the position along the fiber is presented in Fig. 11. In all LF measurements with DAS, the maximum strain amplitude in the PMMA sample did not exceed 3×10^{-8} in the uniaxial experiments and 4×10^{-8} in the experiment with oscillating confining pressure. The ratio R_c (see Eq. (17)) found in the experiment with the confining setup at 1 Hz is equal to 26.8.

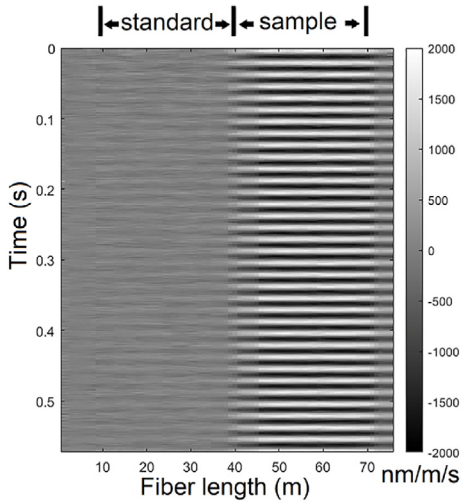

Fig. 5. The data obtained at 60 Hz in the uniaxial experiments and recorded by the Silixa iDASv2 interrogator unit.

4.2. Results of the ultrasonic and low-frequency measurements with strain gauges

Fig. 12 presents Poisson's ratio, Young's modulus, bulk modulus and shear modulus of the PMMA sample obtained at frequencies of 0.1 Hz to 100 Hz and a frequency of 0.5 MPa under a uniaxial pressure of 10 MPa using the FO uniaxial setups with DAS (Figs. 1 and 2) and with strain gauges (Fig. 3), and the ultrasonic setup (Fig. 4). The strain amplitude in the PMMA sample was maintained at the level of 1×10^{-6} in both LF and ultrasonic experiments.

5. Analysis and discussion

As can be seen from Fig. 12a, in the LF experiments with strain gauges, the dispersion of Poisson's ratio at seismic frequencies is virtually negligible. The Poisson's ratio averaged over the frequencies of measurements is 0.318. The Poisson's ratios measured in the LF measurements with DAS at 1 Hz and ultrasonic experiments are equal to 0.314 and 0.326, correspondingly. Thus, the

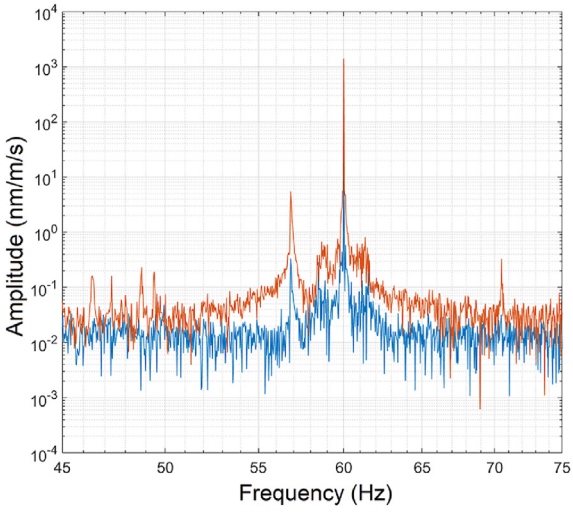

Fig. 6. The spectra of the signals measured with the Silixa iDASv2 interrogator unit. The blue and red lines correspond to the data obtained for the standard and the sample, correspondingly.

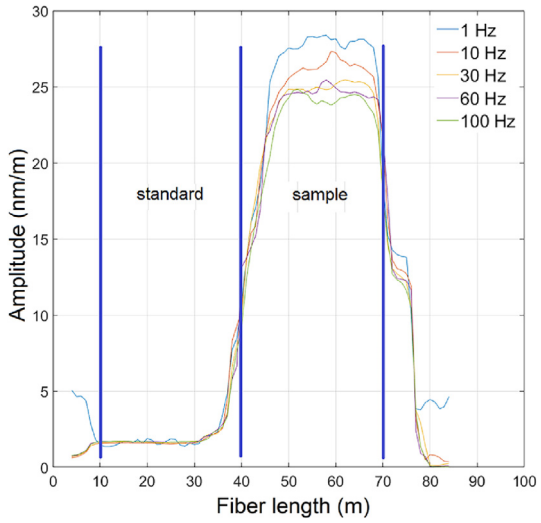

Fig. 7. The profiles of the strain amplitudes obtained at frequencies of 1 Hz to 100 Hz using the Silixa iDASv2 interrogator.

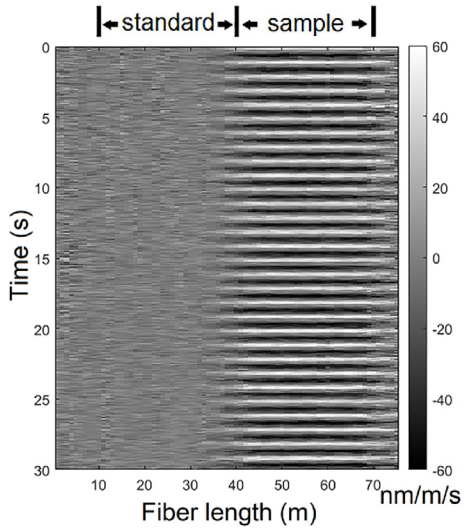

Fig. 9. The data obtained at 1 Hz in the experiment with confining pressure oscillations and recorded by the Silixa iDASv2 unit.

Table 1
The ratio of the radial strain amplitudes in the standard and sample R_u obtained with the Silixa iDASv2 interrogator.

Frequency (Hz)	Ratio R_u
1	18.67
10	16.28
30	15.24
60	14.61
100	14.3

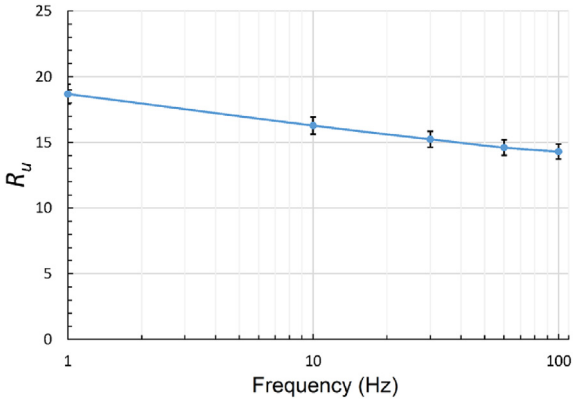

Fig. 8. The dependence of the ratio of the strain amplitudes detected on the sample and the standard on the frequency of axial pressure oscillations measured by the Silixa iDASv2 interrogator.

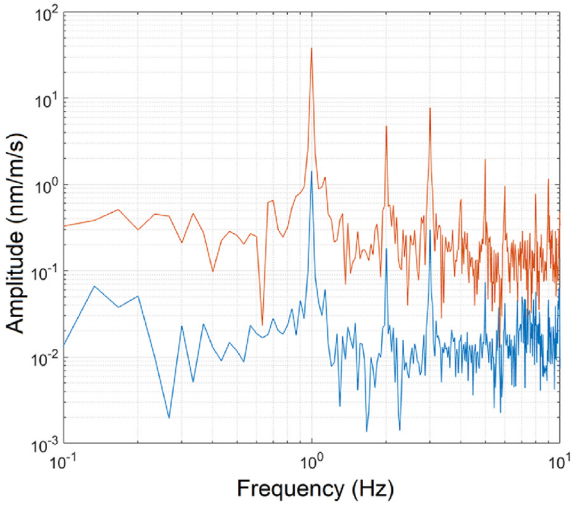

Fig. 10. The frequency dependence of the strain amplitudes obtained with the Silixa iDASv2 interrogator unit. The blue and red lines correspond to the strains in the standard and the sample, correspondingly.

difference in the values of the Poisson's ratio measured at seismic and ultrasonic frequencies does not exceed 3%.

Note that the insignificant frequency dependence of Poisson's ratio of PMMA was experimentally confirmed in a number of studies: in the seismic range from 1 Hz to 100 Hz by Mikhaltsevitch et al. (2021), in the range from 140 Hz to 720 Hz by Giovagnoni (1994), and at frequencies of 1 kHz to 40 kHz by Mousavi et al. (2004).

Given such a negligible dispersion of Poisson's ratio of PMMA, we can use the value obtained at 1 Hz for other seismic frequencies. Fig. 12b shows the LF bulk, Young's and shear moduli derived from Eqs. (11), (17) and (18) using Poisson's ratio at 1 Hz. For comparison, Fig. 12b also presents the elastic moduli obtained at an ultrasonic frequency of 0.5 MHz and at frequencies of 0.1 Hz to 100 Hz using the semiconductor strain gauges.

The obtained data demonstrate a strong rising trend of the elastic moduli with frequency specific for such a viscoelastic material as PMMA, which can be interpreted as a transition between static and dynamic (ultrasonic) moduli (Fjær, 2019).

The literature on laboratory measurements of the dispersion of the elastic moduli of PMMA in the seismic frequency range is relatively scarce, with the published results obtained mostly without applying external pressure to the material. The most common reported values for the elastic moduli of PMMA at the lower (0.1 Hz) and upper (100 Hz) limits of the LF range of our study are as follows: the value interval is between 2.6 GPa and 4.5 GPa for Young's modulus (Koppelmann, 1958; Yee and Takemori, 1982; Ciccotti and Mulargia, 2004; Liao and Wells, 2008; Borgomano et al., 2020), between 1.8 GPa and 5.3 GPa for bulk modulus

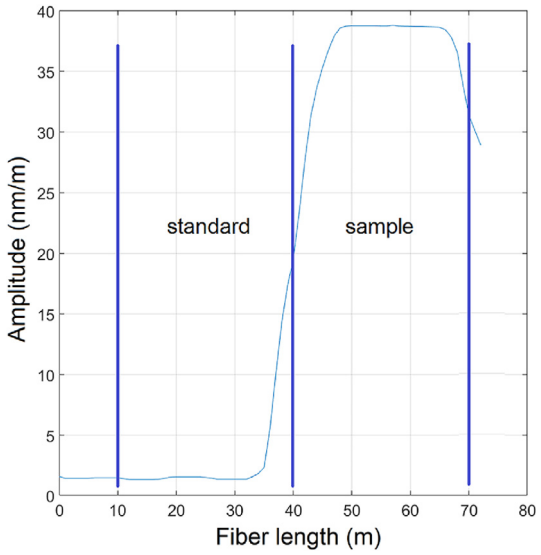

Fig. 11. The dependence of the strain amplitudes on the position along the fiber obtained in the experiment with the confining pressure oscillations at 1 Hz using the Silixa iDASv2 unit.

(Koppelmann, 1958; Yee and Takemori, 1982; Borgomano et al., 2020), and between 1 GPa and 2 GPa for shear modulus (Koppelmann, 1958; Yee and Takemori, 1982; Capodagli and Lakes, 2008; Saltiel et al., 2019). Therefore, the elastic moduli obtained in our LF measurements with DAS and strain gauges are in a good agreement with the literature data.

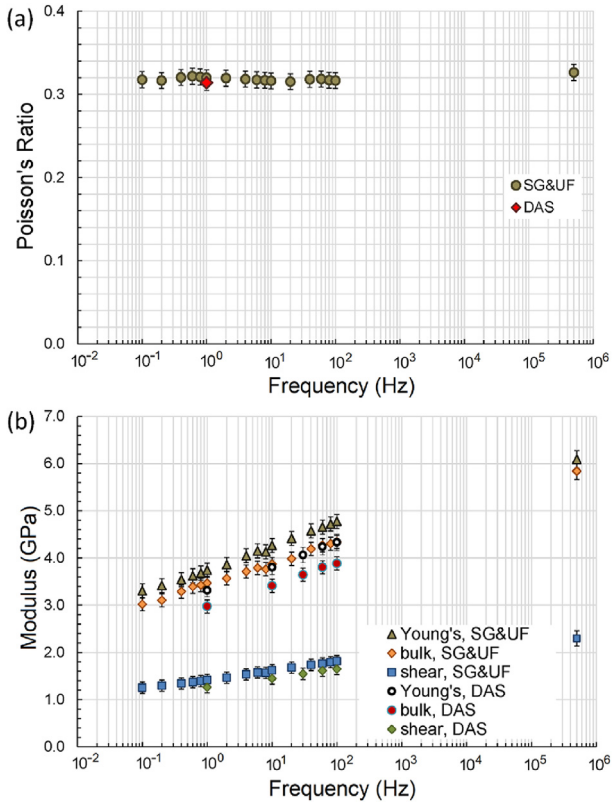

Fig. 12. Poisson's ratio (a), Young's modulus, bulk modulus and shear modulus (b) of the PMMA sample found at seismic and ultrasonic frequencies under a uniaxial pressure of 10 MPa using the FO setup with strain gauges and the uniaxial setup.

The difference within 0.5 GPa between the moduli measured with strain gauges and DAS observed at all frequencies of measurements can be attributed to a two order of magnitude difference in strain amplitudes used for the measurements with DAS and strain gauges (Fjær, 2019). As for example, Ciccotti and Mulargia (2004) found that a static Young's modulus of PMMA is equal to 3.6 GPa, when a quasistatic Young's modulus measured at a frequency of 0.01 Hz is 2.7 GPa. Inasmuch as this result is contrary to the trend of decreasing Young's modulus with decreasing frequency, this difference can be explained by the difference in strain amplitudes, which are equal to 10^{-3} in static measurements and 10^{-5} in quasi-static measurements at 0.01 Hz.

6. Conclusions

We present the results of the laboratory experiments using a new version of the FO method for measuring the elastic properties of solids based on fiber-optic DAS. The method includes FO measurements with DAS acquisition, conducted in turn at uniaxial and confining pressures of the same value, and enables to determine the main elastic parameters of solids, such as Young's modulus, bulk modulus, shear modulus, and Poisson's ratio. To confirm the performance of the new method, laboratory tests were carried out on two specimens, a PMMA sample and an aluminium standard, first under uniaxial pressure at frequencies of 1, 10, 30, 60 and 100 Hz and then under confining pressure at a frequency of 1 Hz. Both pressures were equal to 10 MPa. In all FO measurements with DAS, the maximum strain amplitude in the PMMA sample did not exceed 4×10^{-8}. Given insignificant dispersion of the Poisson's ratio, corroborated by the standard FO measurements with strain gauges at seismic frequencies and ultrasonic measurements at a frequency of 0.5 MHz, the Poisson's ratio obtained at 1 Hz was used to find moduli at other seismic frequencies. The FO measurements with strain gauges and ultrasonic measurements were carried out at strain amplitudes of 1×10^{-6} under a uniaxial pressure of 10 MPa. The results of the FO experiments with DAS are in good agreement with the results obtained using the FO measurements with strain gauges. The difference in the moduli observed in the measurements with strain gauges and DAS does not exceed 0.5 GPa and can be attributed to the two orders of magnitude difference in strain amplitudes used for the measurements with DAS and strain gauges.

The advantages of the proposed FO method with DAS acquisition are associated with a higher strain sensitivity (to 10^{-12}), a higher signal-to-noise ratio and a shorter measurement time in comparison with the standard FO method based on the use of semiconductor strain gauges. The main drawback of the method is related to the fact that to measure the entire range of elastic parameters of the sample, two sets of measurements are required, carried out at both uniaxial and confining pressures. Exploring a new design of the apparatus for obtaining all elastic parameters in one set of measurements is the subject of future research.

Data availability statement

The data that support the findings of this study are available from the corresponding author upon reasonable request.

Declaration of competing interest

The authors declare that they have no known competing financial interests or personal relationships that could have appeared to influence the work reported in this paper.

References

Adelinet, M., Fortin, J., Gueguen, Y., Schubnel, A., Geoffroy, L., 2010. Experimental evidence of frequency and fluid effects in an Icelandic basalt. Geophys. Res. Lett. 37 (2), L02303.

Agrawal, S., Patidar, D., Dixit, M., Sharma, K., Saxena, N., 2010. Investigation of thermo-mechanical properties of PMMA. AIP Conf. Proc. 1249, 79–82.

Baldwin, C.S., 2014. Brief history of fiber optic sensing in the oil field industry. In: Proceedings of SPIE 9098, Fiber Optic Sensors and Applications, vol. XI, 909803.

Barrias, A., Casas, J.R., Villalba, S., 2016. A review of distributed optical fiber sensors for civil engineering applications. Sensors 16 (5), 748.

Becker, M.W., Coleman, T.I., 2019. Distributed acoustic sensing of strain at Earth tide frequencies. Sensors 19 (9), 1975.

Borgomano, J.V.M., Gallagher, A., Sun, C., Fortin, J., 2020. An apparatus to measure elastic dispersion and attenuation using hydrostatic- and axial stress oscillations under undrained conditions. Rev. Sci. Instrum. 91, 034502.

Capodagli, J., Lakes, R., 2008. Isothermal viscoelastic properties of PMMA and LDPE over 11 decades of frequency and time: a test of time–temperature superposition. Rheol. Acta 47, 777–786.

Carneiro, V.H., Puga, H., 2018. Temperature variability of Poisson's ratio and its influence on the complex modulus determined by dynamic mechanical analysis. Technologies 6 (3), 81.

Ciccotti, M., Mulargia, F., 2004. Differences between static and dynamic elastic moduli of a typical seismogenic rock. Geophys. J. Int. 157 (1), 474–477.

Daley, T.M., Miller, D.E., Dodds, K., Cook, P., Freifeld, B.M., 2016. Field testing of modular borehole monitoring with simultaneous distributed acoustic sensing and geophone vertical seismic profiles at Citronelle, Alabama. Geophys. Prospect. 64 (5), 1318–1334.

Damiano, E., Avolio, B., Minardo, A., Olivares, L., Picarelli, L., Zeni, L., 2017. A laboratory study on the use of optical fibers for early detection of prefailure slope movements in shallow granular soil deposits. Geotech. Test J. 40 (4), 529–541.

Fan, L., Bao, Y., Chen, G., 2018. Feasibility of distributed fiber optic sensor for corrosion monitoring of steel bars in reinforced concrete. Sensors 18 (11), 3722.

Fenta, M.C., Potter, D.K., Szanyi, J., 2021. Fibre optic methods of prospecting: a comprehensive and modern branch of Geophysics. Surv. Geophys. 42, 551–584.

Fernandez-Ruiz, M.R., Soto, M.A., Williams, E.F., Martin-Lopez, S., Zhan, Z., Gonzalez-Fjær, E., 2019. Relations between static and dynamic moduli of sedimentary rocks. Geophys. Prospect. 67 (1), 126–139.

Giovagnoni, M., 1994. On the direct measurement of the dynamic Poisson's ratio. Mech. Mater. 17 (1), 33–46.

Gordon, R.B., Davis, L.A., 1968. Velocity and attenuation of seismic waves in imperfectly elastic rock. J. Geophys. Res. 73 (12), 3917–3935.

Gorshkov, B.G., Yüksel, K., Fotiadi, A.A., et al., 2022. Scientific applications of distributed acoustic sensing: state-of-the-art review and perspective. Sensors 22, 1033.

Habel, W.R., Krebber, K., 2011. Fiber-optic sensor applications in civil and geotechnical engineering. Photonic Sens 1 (3), 268–280.

Jackson, I., Schijns, H., Schmitt, D.R., Mu, J., Delmenico, A., 2011. A versatile facility for laboratory studies of viscoelastic and poroelastic behaviour of rocks. Rev. Sci. Instrum. 82, 064501.

Koppelmann, V.J., 1958. Über die bestimmung des dynamischen elastizitätsmoduls und des dynamischen schubmodulus im frequenzbereich von 10^{-5} bis 10^{-1} Hz. Rheol. Acta 1, 20–28 (in German).

Lebedev, M., Pervukhina, M., Mikhaltsevitch, V., Dance, T., Bilenko, O., Gurevich, B., 2013. An experimental study of acoustic responses on the injection of supercritical CO_2 into sandstones from the Otway Basin. Geophysics 78 (4), D293–D306.

Liao, Y., Wells, V., 2008. Estimation of complex Young's modulus of non-stiff materials using a modified Oberst beam technique. J. Sound Vib. 316 (1–5), 87–100.

Linker, R., Klar, A., 2015. Detection of sinkhole formation by strain profile measurements using BOTDR: simulation study. J. Eng. Mech. 143 (3), B4015002.

Liu, Y., Wu, K., Jin, G., Moridis, G., 2020. Rock deformation and strain-rate characterization during hydraulic fracturing treatments: insights for interpretation of low-frequency distributed acoustic-sensing signals. SPE J. 25 (5), 2251–2264.

Lu, P., Lalam, N., Badar, et al., 2019a. Distributed optical fiber sensing: review and perspective. Appl. Phys. Rev. 6 (4), 041302.

Lu, X., Thomas, P.J., Hellevang, J.O., 2019b. A review of methods for fibre-optic distributed chemical sensing. Sensors 19 (13), 2876.

Luo, B., Lellouch, A., Jin, G., Biondi, B., Simmons, J., 2021. Seismic inversion of shale reservoir properties using microseismic-induced guided waves recorded by distributed acoustic sensing. Geophysics 86 (4), R383–R397.

Ma, J., Pei, H., Zhu, H., Shi, B., Yin, J., 2023. A review of previous studies on the applications of fiber optic sensing technologies in geotechnical monitoring. Rock Mech. Bull. 2 (1), 100021.

Mavko, G., 1979. Frictional attenuation: an inherent amplitude dependence. J. Geophys. Res. Solid Earth 84 (B9), 4769–4775.

Mikhaltsevitch, V., Lebedev, M., Chavez, R., Vargas Jr., E.A., Vasquez, G.F., 2021. A laboratory forced-oscillation apparatus for measurements of elastic and anelastic properties of rocks at seismic frequencies. Front. Earth Sci. 9, 654205.

Mikhaltsevitch, V., Lebedev, M., Gurevich, B., 2014a. A laboratory study of low-frequency wave dispersion and attenuation in water-saturated sandstones. Lead. Edge 33 (6), 616–622.

Mikhaltsevitch, V., Lebedev, M., Gurevich, B., 2014b. Measurements of the elastic and anelastic properties of sandstone flooded with supercritical CO_2. Geophys. Prospect. 62 (6), 1266–1277.

Mohamad, H., Soga, K., Pellew, A., 2011. Performance monitoring of a secant piled wall using distributed fibre optic strain sensing. J. Geotech. Geoenviron. Eng. 137 (12), 1236–1243.

Mousavi, S., Nicolas, D.F., Lundberg, B., 2004. Identification of complex moduli and Poisson's ratio from measured strains on an impacted bar. J. Sound Vib. 277 (4–5), 971–986.

Murayama, H., Kageyama, K., Naruse, H., Shimada, A., Uzawa, K., 2003. Application of fiber-optic distributed sensors to health monitoring for full-scale composite structures. J. Intell. Mater. Syst. Struct. 14 (1), 3–13.

Nourifard, N., Lebedev, M., 2019. Research note: the effect of strain amplitude produced by ultrasonic waves on its velocity. Geophys. Prospect. 67, 715–722.

Ohno, H., Naruse, H., Kihara, M., Shimada, A., 2001. Industrial applications of the BOTDR optical fiber strain sensor. Opt. Fiber Technol. 7, 45–64.

Ògúnsànmì, A., Jackson, I., Borgomano, J.V., Fortin, J., Sidi, H., Gerhardt, A., Gurevich, B., Mikhaltsevitch, V., Lebedev, M., 2021. Elastic properties of a reservoir sandstone: a broadband inter-laboratory benchmarking exercise. Geophys. Prospect. 69 (2), 404–418.

Pevzner, R., Glubokovskikh, S., Isaenkov, R., et al., 2022. Monitoring subsurface changes by tracking direct-wave amplitudes and travel times in continuous DAS VSP data. Geophysics 87 (1), A1–A6.

Rehman, S., Mendez, A., 2012. Optical fibers present opportunities and challenges for geophysical applications. Offshore Mag 72 (3), 1–5.

Rossi, M., Wisén, R., Vignoli, G., Coni, M., 2022. Assessment of distributed acoustic sensing (DAS) performance for geotechnical applications. Eng. Geol. 306 (5), 106729.

Saltiel, S., Selvadurai, P.A., Bonner, B.P., Glaser, S.D., Ajo-Franklin, J.B., 2019. Experimental development of low-frequency shear modulus and attenuation measurements in mated rock fractures: shear mechanics due to asperity contact area changes with normal stress. Geophysics 82 (2), M19–M36.

Sidenko, E., Tertyshnikov, K., Bona, A., Pevzner, R., 2021. DAS-VSP interferometric imaging: CO2CRC Otway Project feasibility study. Interpretation 9 (4), SJ1–SJ12.

Subramaniyan, S., Quintal, B., Tisato, N., Saenger, E.H., Madonna, C., 2014. An overview of laboratory apparatuses to measure seismic attenuation in reservoir rocks. Geophys. Prospect. 62 (6), 1211–1223.

Suo, W., Lu, Y., Shi, B., Zhu, H., Wei, G., Jiang, H., 2016. Development and application of a fixed-point fiber-optic sensing cable for ground fissure monitoring. J. Civil Struct. Health Monit. 6 (4), 715–724.

Tejedor, J., Macias-Guarasa, J., Martins, H.F., et al., 2018. Real field deployment of a smart fiber-optic surveillance system for pipeline integrity threat detection: architectural issues and blind field test results. J. Lightwave Technol. 36 (4), 1052–1062.

Tschoegl, N.W., Knauss, W.G., Emri, I., 2002. Poisson's ratio in linear viscoelasticity – a critical review. Mech. Time-Dependent Mater. 6 (1), 3–51.

Udd, E., 1995. An overview of fiber-optic sensors. Rev. Sci. Instrum. 66 (8), 4015–4030.

Winkler, K., Nur, A., Gladwin, M., 1979. Friction and seismic attenuation in rocks. Nature 277, 528–531.

Xie, T., Shi, B., Zhang, C.-C., et al., 2021. Distributed acoustic sensing (DAS) for geomechanics characterization: a concise review. IOP Conf. Ser. Earth Environ. Sci. 861 (4), 042033.

Xu, D.-S., Yin, J.-H., 2016. Analysis of excavation induced stress distributions of GFRP anchors in a soil slope using distributed fiber optic sensors. Eng. Geol. 213 (4), 55–63.

Yee, A.F., Takemori, M.T., 1982. Dynamic bulk and shear relaxation in glassy polymers. I: experimental techniques and results on PMMA. J. Polym. Sci. 20, 205–224.

Yurikov, A., Pevzner, R., Tertyshnikov, K., Mikhaltsevitch, V., Gurevich, B., Lebedev, M., 2021. Laboratory measurements with DAS: a fast and sensitive tool to obtain elastic properties at seismic frequencies. Lead. Edge 40 (9), 655–661.

Zhang, S., Das, A., 2021. HandLock: enabling 2-FA for smart home voice assistants using inaudible acoustic signal. In: Proceedings of RAID'21: 24th International Symposium on Research in Attacks, Intrusions and Defenses. San Sebastian, Spain, pp. 251–265.

Zhu, H.-H., Liu, W., Wang, T., Su, J.-W., Shi, B., 2022. Distributed acoustic sensing for monitoring linear infrastructures: current status and trends. Sensors 22 (19), 7550.

Vassily Mikhaltsevitch holds a MS degree (obtained in 1982) and a PhD in Physics/Mathematics (1997) from Kaliningrad State University, Russia, and a PhD degree in Geophysics (2017) from Curtin University, Australia. From 1982 to 1998, he worked as a Senior Research Scientist, Assistant Professor and Laboratory Supervisor at the Department of Quantum Radiophysics of Kaliningrad State University. From 1998 to 2008, Dr. Mikhaltsevitch was a Senior Research Scientist with QRSciences, a research and development company focused on using Nuclear Quadrupole Resonance to advance technologies for border security. In 2008–2010 he was a Senior Analyst in Core Laboratory of Australia. Since April 2010, Dr. Mikhaltsevitch is affiliated as academic staff with Curtin University. Now he is a Senior Research Fellow in the School of Earth and Planetary Sciences at Curtin University. His current research interests are in experimental rock physics, in particular low-frequency measurements. He is the inventor of 23 international patents, has published 50 peer-reviewed papers and presented his research and contributed to research projects nationally and internationally.